

Supporting Information

Energy transfer mediated by asymmetric hydrogen-bonded interfaces

Elizabeth R. Young, Joel Rosenthal and Daniel G. Nocera*

*Department of Chemistry, 6-335, Massachusetts Institute of Technology, 77 Massachusetts Avenue,
Cambridge, MA 02139-4307*

nocera@mit.edu

<i>Index</i>	<i>Page</i>
Experimental: synthesis	S2
Experimental: Physical measurements and methods	S5
Excited state properties	S9
Förster Resonant Energy Transfer (FRET) calculation	S10
Table S1. Spectral fits and parameters derived therefrom	S12
Table S2. FRET calculation parameters and values	S13
Figure S1. Spectral shifts with deprotonation of the amidinium	S14
Figure S2. Benesi-Hildebrand plots for deprotonation of 3 and 9	S15
Figure S3. Differential pulse voltammetry for Ru^A , Ru^B , 3 , 5 , and 9 in CH ₂ Cl ₂	S16
Figure S4. Differential pulse voltammetry for Ru^A , Ru^B , 3 in THF	S17
Figure S5. Variable temperature emission spectra	S18
Figure S6. Temperature-dependence of emission lifetimes for Ru^A and Ru^B	S19
Figure S7. Spectra used for FRET calculations	S20

Experimental

Synthesis

Materials. Phenyl cyanate (PhOCN),¹ 4'-Methyl-2,2'-bipyridine-4-carboxylic acid (bpy-COOH),² [*bis*(2,2'-bipyridine)ruthenium(II)(bpy-COOH)](PF₆)₂ (**Ru^B**),³ and *bis*(4,4'-*bis*(trifluoromethyl)-2,2'-bipyridine)ruthenium(II) dichloride (Ru(bt₃fmbpy)₂Cl₂)⁴ were prepared as described previously. Bromoferrocene (**1**) was purchased from Sigma-Aldrich and used as received.

Cyanoferrocene (2). Bromoferrocene (**1**) (400 mg, 1.365 mmol) is placed in a 50 mL Schlenk tube, which is evacuated and filled with 10 mL of dry THF. The reaction vessel was then evacuated and backfilled with N₂ three times. The reaction solution was cooled to -78 °C and 0.5 mL of 3.3 M CH₃Li in ether (1.65 mmol) was added using an airtight syringe. The reaction was stirred at -78 °C for 3.5 h at which point 0.6 mL (5.6 mmol) of PhOCN was added. The reaction was stirred at -78 °C for 1 h and was allowed to slowly warm to room temperature over the course of several hours. To quench the reaction, 30 mL of 6 N NaOH was added to the orange solution and the resultant mixture was extracted three times with 40 mL of ether. The ethereal extracts were combined and washed twice with brine and water. The organic layer was then separated, dried over Na₂SO₄ and concentrated in vacuo. Chromatography of the product on silica using hexanes and CH₂Cl₂ (3:1) as the eluent delivered 223 mg of the title compound as a yellow microcrystalline solid in 68% yield. ¹H NMR (300 MHz, CDCl₃, 25 °C), δ/ppm: 4.66 (t, J = 1.2 Hz, 2H), 4.39 (t, J = 1.2 Hz, 2H), 4.34 (s, 5H). HREIMS [M]⁺, m/z: Calcd for C₁₁H₉FeN, 211.0079. Found, 211.0082.

Amidiniumferrocene chloride (3). Cyanoferrocene (**2**) (100 mg, 0.417 mmol) was placed in a 100 mL Schlenk flask, which was evacuated. To the vessel was added 20 mL of dry toluene. The resulting dark yellow solution was backfilled with N₂ and heated to 90 °C with stirring. Chloromethylaluminum amide (4.0 mL, 1.2 M in toluene)⁵ was added to the heated solution and stirring was continued for an additional 40 h (at 90 °C under N₂), after which, heating was discontinued and the reaction solution was poured onto a slurry of silica and CHCl₃. The mixture was stirred under air for 5 – 10 min and filtered through

-
1. R. A. Moss, G. Chu, R. R. Sauers, *J. Am. Chem. Soc.*, 2005, **127**, 2408-2409.
 2. D. G. McCafferty, B. M. Bishop, C. G. Wall, S. G. Hughes, S. L. Mecklenberg, T. J. Meyer, B. W. Erickson, *Tetrahedron*, 1995, **51**, 1093-1106.
 3. J. A. Roberts, J. P. Kirby, D. G. Nocera, *J. Am. Chem. Soc.*, 1995, **117**, 8051-8052.
 4. M. Furue, K. Maruyama, T. Oguni, M. Naiki, M. Kamachi, *Inorg. Chem.*, 1992, **31**, 3792-3795.
 5. J. I. Levin, E. Tuross, S. M. Weinreb, *Synth. Commun.* 1982, **12**, 989-993.

sintered glass. The filtercake was rinsed with 25% CH₃OH in CH₃CN until the eluent was colorless. The filtrate was combined and concentrated in vacuo. Purification was accomplished by column chromatography on silica using CH₂Cl₂ to remove nonpolar impurities and 5% CH₃OH in CH₂Cl₂ to isolate the title compound (106 mg) in 87% yield. ¹H NMR (300 MHz, DMSO-*d*₆, 25 °C), δ/ppm: 8.76 (br s, 4H), 5.18 (s, 2H), 4.66 (s, 2H), 4.28 (s, 5H). HRESIMS [M – HCl]⁺, m/z: Calcd for C₁₃H₁₈ClFeN₂, 228.0344. Found, 228.0337.

4-Cyanophenylferrocene (4). In a 100 mL Schlenk flask were combined 260 mg (0.887 mmol) of bromoferrocene (**3**), 220 mg (1.49 mmol) of 4-cyanophenyl boronic acid and 140 mg (0.191 mmol) of Pd(dppf)Cl₂. The reaction vessel was evacuated and backfilled with N₂. To the mixture of reactants was added 40 mL of THF and water (3:1) that had been sparged with N₂ for 45 min. The resulting solution was stirred and heated at reflux under N₂ for 16 h, after which time the reaction was cooled to room temperature. The red solution was extracted twice with 100 mL of CH₂Cl₂ and the organic extracts were subsequently combined and washed three times with 50 mL of water. After drying the orange solution over Na₂SO₄, the desired product was isolated as an orange microcrystalline solid (236 mg, 84% yield) using a silica column with CH₂Cl₂ and hexanes as the eluent (3:1). ¹H NMR (300 MHz, CDCl₃, 25 °C), δ/ppm: 7.56 (d, J = 4.5 Hz, 2H), 7.53 (d, J = 4.5 Hz, 2H), 4.70 (t, J = 1.4 Hz, 2H), 4.44 (d, J = 1.4 Hz, 2H), 4.06 (s, 5H). HRESIMS [M]⁺, m/z: Calcd for C₁₇H₁₃FeN, 287.0392. Found, 287.0393.

4-Amidiniumphenylferrocene chloride (5). Starting with 105 mg of **4** (0.366 mol), the title compound was prepared in a manner identical to that described for **3**, above. The reaction generated 113 mg of the title compound in 92% yield. ¹H NMR (300 MHz, DMSO-*d*₆, 25 °C), δ/ppm: 9.17 (br s, 4H), 7.76 (d, J = 2.9, 2H), 7.74 (d, J = 2.9, 2H), 4.96 (t, J = 0.8 Hz, 2H), 4.47 (t, J = 0.8 Hz, 2H), 4.12 (s, 5H). HRESIMS [M – Cl]⁺, m/z: Calcd for C₁₇H₁₇FeN₂, 305.0736. Found, 305.0729.

Trimethylsilylethynylferrocene (6). A mixture of bromoferrocene (**1**) 260 mg (0.887 mmol), PdCl₂(PPh₃)₂ (50 mg 0.070 mmol) and CuI (10 mg, 0.050 mmol) were combined in a 50 mL Schlenk flask. The flask was evacuated and backfilled with N₂. To the mixture was added 15 mL of dry DMF and NEt₃ (1:1). The solution was heated to 110 °C under N₂ and 1.0 mL of (trimethylsilyl)acetylene was added to the stirred solution. After 24 h, the reaction was cooled to room temperature and the solvent was removed under reduced pressure. The crude material was dissolved in CH₂Cl₂, washed twice with water (75 mL) and the organic layer was dried over Na₂SO₄. The crude material was then purified on silica using hexanes as the eluent to generate 212 mg of the title compound in 77% yield. ¹H NMR (300 MHz, CDCl₃, 25 °C), δ/ppm: 4.45 (t, J = 1.1 Hz, 2H), 4.07 (s, 5H), 3.87 (t, J

= 1.1 Hz, 2H), 0.36 (s, 9H). HREIMS $[M]^+$, m/z : Calcd for $C_{17}H_{23}FeSi$, 311.0918. Found, 311.0909.

Ethynylferrocene (7). The trimethylsilyl-protected alkynyl ferrocene (**6**) (200 mg, 0.643 mmol) was dissolved in 12 mL of THF and CH_3OH (3:1) and 100 mg (0.1 mol) of K_2CO_3 was added to the stirred solution. The resulting mixture was stirred for 18 h under air. To the mixture was added 25 mL of saturated NH_4Cl and 20 mL of CH_2Cl_2 . The organic layer was separated, washed twice with 20 mL of saturated NH_4Cl and dried over Na_2SO_4 . The resulting solution was filtered through a short plug of silica and concentrated under reduced pressure. Chromatography on silica, using hexanes as the eluent delivered the desired product (97 mg) in 72% yield. 1H NMR (300 MHz, $CDCl_3$, 25 °C), δ/ppm : 4.78 (t, J = 1.0 Hz, 2H), 4.52 (t, J = 1.0 Hz, 2H), 4.26 (s, 5H). HREIMS $[M]^+$, m/z : Calcd for $C_{12}H_{10}Fe$, 210.0132. Found, 210.0134.

Cyanoethynylferrocene (8). A solution of ethynylferrocene (**7**) (930 mg, 4.43 mmol) in THF (30 mL) was cooled to -78 °C under an atmosphere of N_2 . To the orange solution was added 3.5 mL of 1.6 M $n-BuLi$ in hexane (5.6 mmol) and the solution was stirred for 90 min. $PhOCN$ (1.0 mL) was injected into the stirred solution and the reaction was allowed to warm to room temperature over the course of several hours. To the resulting orange solution was added 50 mL of 1 M $NaOH$ and the biphasic mixture was extracted twice with 100 mL of ether. The combined ethereal layers were washed twice each with brine and water. The orange ethereal solution was then dried over Na_2SO_4 and concentrated under reduced pressure. The desired product was purified by chromatography on silica using hexanes and CH_2Cl_2 (5:1) as the eluent to generate 853 mg of the title compound in 82% yield. 1H NMR (300 MHz, $CDCl_3$, 25 °C), δ/ppm : 4.64 (t, J = 1.0 Hz, 2H), 4.41 (t, J = 1.0 Hz, 2H), 4.31 (s, 5H). HREIMS $[M]^+$, m/z : Calcd for $C_{13}H_9FeN$, 235.0084. Found, 235.0076.

Amidiniumethynylferrocene chloride (9). Starting with 70 mg of **8** (0.298 mol), the title compound was prepared in a manner identical to that used for **3**, above. The reaction generated 63 mg of the title compound in 83% yield. 1H NMR (300 MHz, $DMSO-d_6$, 25 °C), δ/ppm : 9.27 (br s, 4H), 4.70 (t, J = 0.8 Hz, 2H), 4.55 (t, J = 0.8 Hz, 2H), 4.36 (s, 5H). HRESIMS $[M - Cl]^+$, m/z : Calcd for $C_{13}H_{13}FeN_2$, 253.0423. Found, 253.0433.

$[Ru(btmbpy)_2(bpy-COOH)](PF_6)_2$ (Ru^A). $Ru(btmbpy)_2Cl_2$ (200 mg, 0.264 mmol, 1 eq) and $bpy-COOH$ (60 mg, 1.06 eq) were combined in a 100 mL round bottom flask along with 50 mL of 70% ethanol. The mixture was heated at reflux for 1 h, at which point 60 mg more of the $bpy-COOH$ ligand was added. The mixture was heated at reflux for seven more

hours and the solvent removed in vacuo. The residue was dissolved in ~30 mL of water, acidified to pH 1 with 60% HPF₆, and solid NH₄PF₆ was added to induce precipitation. The dark red-purple precipitate was isolated by filtration over a fine glass frit and washed with cold water and ether. The product was recrystallized from acetone/ether and isolated as a red solid (260 mg, 83 % yield). ¹H NMR (300 MHz, d-acetone, 25 °C) δ = 2.63 (s, 3H, bpy-CH₃), 7.44-9.52 (m, 18H).

Physical measurements and methods

¹H NMR spectra were recorded at 25 °C in the MIT DCIF on a Varian XL-500, Unity 300 or Mercury 300 spectrometer. All chemical shifts are reported using the standard δ notation in parts-per-million; positive chemical shifts are to higher frequency from the given reference. Absorption spectra were obtained using a Spectral Instruments 440 Series spectrophotometer. Steady-state emission spectra were recorded on an automated Photon Technology International (PTI) QM 4 fluorimeter equipped with a 150 W Xe arc lamp and a Hamamatsu R928 photomultiplier tube. Time-resolved emission (TE) and transient absorption (TA) measurements were performed with pump light provided by the third harmonic (355 nm) of the 1064-nm fundamental of a pulsed Nd:YAG laser (Spectra-Physics Quanta-Ray PRO-Series). The third harmonic is used to pump an optical parametric oscillator (OPO) at a repetition rate of 10 Hz with pulse energies of ~340 mJ/pulse and pulse width of ~7 ns. This Spectra-Physics laser has been integrated into an experimental set-up for time-resolved emission and absorption studies described elsewhere.⁶ Variable-temperature time resolved emission spectroscopy was performed using as the excitation source a chirped-pulse amplified Ti:Sapphire laser system that has been described elsewhere.⁶ In this experiment, the 100-fs, 800-nm output of the regenerative amplifier was frequency-doubled in a visible optical parametric amplifier (BMI Alpha-1000) to produce a 1 kHz pulse train of excitation pulses at 400 nm for resonant excitation of the MLCT band of **Ru^A** and **Ru^B**. The excitation was vertically polarized and attenuated to 50 - 250 nJ/pulse. Variable-temperatures were achieved using a modular cryogenic refrigeration system (Air Products and Chemicals) consisting of a single stage helium compressor (model 1R02A) connected via hoses to an expander module (model DE-202) with a heating element and temperature controller (Scientific Instruments, 9600-5) that was interfaced with a custom-made computer program in order to automate the temperature control settings. The expander module is housed within in laboratory interface (model DMX-1) consisting of a vacuum shroud with glass windows for

6. Z.-H. Loh, S. E. Miller, C. J. Chang, S. D. Carpenter, D. G. Nocera, *J. Phys. Chem. A*, 2002, **106**, 11700-11708.

fluorescence spectroscopy in a right-angle configuration and is continuously pumped to maintain a vacuum ($\sim 10^{-4}$ Torr). An ampoule containing the sample is mounted on a copper block and the thermocouple was calibrated with three temperatures: liquid nitrogen (77 K), an ice bath (273 K) and ambient temperature (293 K).

Absorption spectroscopy titrations with **3**, **5** and **9** are shown in Figure S1. The Benesei-Hildebrand plots that accompany these data are shown in Figure S2. These titrations were recorded in a high-vacuum cell comprising a 1-cm pathlength clear fused-quartz cuvette (Starna cells) connected to a 10-cm³ solvent reservoir via a graded seal. High-vacuum Teflon valves were used to seal the cell from the environment and the cuvette from the solvent reservoir. Titrations with a base of known pK_a in CH₃CN were monitored by UV-visible spectroscopy to determine the acidity constants for **3**, **5**, and **9** in CH₃CN. Titrations on **3** were performed at 270 μ M yielding an absorption of 0.312 AU at 231 nm, titrations on **5** were performed at 240 μ M yielding absorptions of 0.456 AU and 0.232 AU at 373 nm and 464 nm, respectively, and experiments on **9** were performed at 670 μ M yielding absorptions of 1.33 AU and 0.643 AU at 355 nm and 464 nm, respectively. High concentrations of **3**, **5**, and **9** were required for UV-visible experiments due to small extinction coefficients for the three ferrocene compounds: $\epsilon_{321}(\mathbf{3}) = 1,180 \text{ M}^{-1} \text{ cm}^{-1}$, $\epsilon_{373}(\mathbf{5}) = 1,900 \text{ M}^{-1} \text{ cm}^{-1}$ and $\epsilon_{355}(\mathbf{9}) = 1,980 \text{ M}^{-1} \text{ cm}^{-1}$. Sample preparation was performed under high-vacuum. An aliquot of **3**, **5**, or **9** (8.4×10^{-6} moles, **3**; 7.19×10^{-7} moles, **5**; and 2.1×10^{-6} moles, **9**) was added to the cuvette and the cell was evacuated under high-vacuum (10^{-5} torr), thereby removing the transferring solvent. Three milliliters of dry CH₃CN were vacuum transferred to the solvent reservoir and subject to three cycles of freeze-pump-thaw. The cell was sealed to the environment and removed from the high vacuum manifold. A titration with 4-dimethylaminopyridine (DMAP) was performed to monitor the spectral shifts associated with deprotonation of the amidinium proton. Prior to each addition of DMAP, the CH₃CN was vacuum transferred to the cuvette with a dry ice/acetone bath and sealed from the solvent reservoir and environment. This procedure ensured that the solvent volume remained constant throughout the course of the experiment. A stock solution of DMAP was added to the open solvent reservoir, while preserving the vacuum in the cuvette, and the transferring solvent was removed with a high vacuum manifold (10^{-5} torr). The solvent reservoir was then sealed from the environment and opened to the cuvette compartment to introduce each new addition of DMAP.

Electrochemical measurements were performed with a Bioanalytical Systems (BAS) Model CV-50W potentiostat/galvanostat. Differential pulse voltammetry (DPV) was performed using a glassy carbon working electrode, a Ag/AgCl reference electrode and a platinum wire auxiliary electrode. DPV traces of **3**, **5**, **9**, **Ru^A**, and **Ru^B** are shown in Figure

S3. The DPV experiments were performed in CH_2Cl_2 with 0.1 M tetrabutylammonium perchlorate $(\text{Bu}_4\text{N})\text{ClO}_4$ as the supporting electrolyte. Concentrations of ~ 1 mM were prepared for DPV experiments on **3**, **5**, **9**, **Ru^A**, and **Ru^B**. A scan rate of 100 mV/sec and a sensitivity of 10 $\mu\text{A}/\text{V}$ were used for data acquisition. Prior to each DPV, argon was bubbled through the solution to remove dissolved O_2 . All potentials are reported versus an internal standard of Fc^+/Fc .

Additional electrochemical measurements were performed on **Ru^A** and **Ru^B** to determine the effects of forming the $---[\text{H}^+]---$ interface on the electrochemical behavior of the complexes. These DPV traces are shown in Figure S4. Because amidine-carboxylic acid binding only occurs in dry, aprotic solvents, all experiments were performed in a dry box using a micro-electrochemical cell (BASi Low Volume Cell for C-2 Cell Stand). Limitations imposed by the low volume cell precluded use of CH_2Cl_2 as the solvent for these measurements. Instead, dry THF was employed as the solvent. DPV scans were performed for the oxidative and reductive waves of **Ru^A** and **Ru^B** and for the oxidation wave of **3** using a glassy carbon working electrode, a Ag/AgNO_3 reference electrode and a platinum wire auxiliary electrode in 0.1 M tetrabutylammonium hexafluorophosphate $(\text{Bu}_4\text{N})\text{PF}_6$ supporting electrolyte. Concentrations of ~ 0.3 mM of **Ru^A**, **Ru^B** and **3** were prepared for the DPV experiments in THF. Addition of phenylamidine (**Ph-am**) was performed, up to 30 eq for **Ru^A** and 50 eq for **Ru^B**, to monitor the electrochemical response of **Ru^A** and **Ru^B** upon binding to the carboxylic acid functionality.

Ambient-temperature time-resolved emission quenching experiments were performed at concentrations of 3.3 μM of **Ru^A** and **Ru^B** and 33 μM of **3**, **5** and **9**. One aliquot of **Ru^A** or **Ru^B** (1×10^{-8} moles) was added to the cuvette and 10 equiv of **3**, **5** or **9** (1×10^{-7} moles) were added to the solvent reservoir. The cell was evacuated under high-vacuum (10^{-5} torr), thereby removing the transferring solvent, but allowing the two compounds to remain separated. Three milliliters of dry CH_2Cl_2 were added to the solvent reservoir and subject to three cycles of freeze–pump–thaw. The cell was sealed to the environment and removed from the high vacuum manifold. Time-resolved emission experiments were first performed on unbound **Ru^A** (or **Ru^B**) under vacuum. Subsequently, the Teflon stopper between the cuvette and solvent reservoir was open and the two compounds were mixed while maintaining vacuum inside the cell. MLCT excitation of **Ru^A** (or **Ru^B**) was performed with 460-nm photons and the emission decay profile was recorded at 640 nm.

Variable-temperature time-resolved and steady-state emission experiments (Figures S5 and S6, respectively) were performed following a sample preparation method

described previously.⁷ One aliquot of **Ru^A** or **Ru^B** (1×10^{-7} moles) and 10 or 5 equiv of **Ph-am** or **3** (1×10^{-6} moles) were added to a borosilicate short-stem glass ampoule (Kimble-Kontes) using a minimum amount of transferring solvent. The neck of the ampoule had been stretched with a flame to reduce the diameter and allow for easier sealing after high vacuum manipulations. The ampoule containing the sample was attached to a high vacuum adaptor. The transferring solvents were removed on a high vacuum manifold ($< 10^{-6}$ Torr) and the sample remained under vacuum for at least 2 h to remove any residual water. One milliliter of dry CH_2Cl_2 was added to the ampoule by vacuum transfer and was subject to at least three cycles of freeze-pump-thaw. The ampoule was then flame-sealed while the solvent remained frozen. The high-vacuum manipulations were necessary to ensure that the samples remained free from exposure to the environment or water, which disrupts the hydrogen bonding between the dyads.

Luminescence lifetime measurements were performed on a Hamamatsu C4334 Streak Scope streak camera that has been described elsewhere.⁶ The emission was collected over a 140-nm window centered on the emission peak. A 1- μs , 2- μs or a 5- μs time base was used. Data acquisition was automated for the variable-temperature experiments. The temperature controller and streak camera were synchronized to enable data collection throughout the entire temperature range. Luminescence experiments lasting approximately 20 min were followed by a 20 min wait time during which the temperature was adjusted and the sample was allowed to equilibrate. This cycle occurred for all of the temperature data points, which were 20 K apart. Each sample was cycled through the entire temperature range 4 times in different sequences to ensure that the data was independent of the sequence.

Temperature-dependent lifetimes of **Ru^A** or **Ru^B** alone and bound to **3** were measured over a temperature range of 200-300 K (Figure S5). Experiments were repeated at least 3 times with newly prepared samples. Luminescence lifetimes were determined from streak camera data analysis by integrating 30-nm slices of the emission peak centered at 660 nm, for **Ru^A** or **Ru^B** respectively, and fitting to a monoexponential decay function. Temperature-dependent lifetimes of **Ru^A:3** or **Ru^B:3** were measured at the same temperature points and the data was fit in the same manner, except that the data was fit to a biexponential decay function with the longer lifetime component fixed to the lifetime obtained from the control experiment, **Ru^A** or **Ru^B**, at each temperature.

7. J. M. Hodgkiss, N. H. Damrauer, S. Pressé, J. Rosenthal, D. G. Nocera, *J. Phys. Chem. B*, 2006, **110**, 18853-18858.

Excited State Properties

The excited state properties of Ru(II) complexes can be deduced from temperature dependent emission spectra (Figure S5). Excited state driving force for emission quenching originates from the MLCT-excited state of **Ru^A** and **Ru^B**. Spectral changes are observed for **Ru^A** (or **Ru^B**) upon addition of **Ph-am** or **3** and upon variations in temperature (Figure S6) necessitating analysis and comparison of both sets of dyads. Absorption of **Ru^A** (or **Ru^B**) occurs into the singlet state, however emission occurs from the triplet state. For this reason, simple overlap of absorption and emission spectra as predicted by the Franck-Condon principle cannot be used for estimating the excited state energy and a more rigorous fitting method is required. To elucidate the excited state energy, emission spectra were fit by the single mode Franck-Condon functional form shown in Eq 1, as described previously by Claude and Meyer:⁸

$$I(\bar{\nu}) = \sum_{v_m=0}^5 \left\{ \left(\frac{E_{00} - v_M \hbar \omega_M}{E_{00}} \right)^3 \cdot \left(\frac{S_M^{v_M}}{v_M!} \right) \times \exp \left[-4(\ln 2) \left(\frac{\bar{\nu} - E_{00} + v_M \hbar \omega_M}{\Delta \bar{\nu}_{0,1/2}} \right)^2 \right] \right\} \quad (1)$$

This spectral fitting method yields the zero-point energy of the ³MLCT state (E_{00}), the electron-vibrational coupling constant (S_M), the vibrational spacing ($\hbar \omega_M$), and the bandwidth ($\Delta \bar{\nu}_{0,1/2}$). The energies of the ³MLCT excited states in **Ru^A** and **Ru^B** can then be determined using the following relations:^{8,9}

$$\Delta G_{es}^0 = E_{00} + \lambda_0 \quad (2)$$

$$\lambda_0 = (\Delta \bar{\nu}_{0,1/2})^2 (16k_B T \ln 2) \quad (3)$$

where the excited state energy (ΔG_{es}^0) is determined by the energy of the luminescence maximum (E_{00}) and the solvent reorganization energy (λ_0) containing low-frequency modes, which are treated classically and related to the full width at half-maximum ($\Delta \bar{\nu}_{0,1/2}$) for a single vibronic component. Conversion of spectroscopic energy to free energy is reasonable because of negligible pressure-volume work and small electronic entropic contributions accompanying excited state production.^{9,10} Corrected emission spectra were

8. K. A. Opperman, S. L. Mecklenburg, T. J. Meyer, *Inorg Chem.*, 1994, **33**, 5295-5301.

9. J. P. Kirby, J. A. Roberts, D. G. Nocera, *J. Am. Chem. Soc.*, 1997, **119**, 9230-9236.

10. J. T. Hupp, G. A. Neyhard, T. J. Meyer, E. M. Kober, *J. Phys. Chem.*, 1992, **96**, 10820-10830.

fit to a standard Franck-Condon functional form^{11,12} to yield fitted values for E_{00} , $\hbar\omega_M$, $\Delta\bar{\nu}_{0,1/2}$ listed in Table S2. Eq 2 and 3 furnish ΔG_{es}^0 for each of the four dyads.

Förster Energy Transfer Calculation

Experimental determination of the quenching rate allows one possible quenching mechanism to be addressed. The viability of FRET transfer is considered in this section for these D-A systems. The intramolecular D-A systems in these studies are separated by a rigid spacer, and thereby lend themselves well to analysis with FRET theory. The rate of FRET is expressed as follows¹³:

$$k_{ET}(\text{Förster}) = \frac{1}{\tau_f} \left(\frac{R_0}{r} \right)^6 \quad (4)$$

where τ_f is the decay time of the fluorescent species in the absence of quencher, r is the donor-to-acceptor distance, and R_0 is the Förster distance, which is defined as the distance at which energy transfer efficiency is 50%. R_0 is defined as,

$$R_0^6 = \frac{900(\ln 10)\kappa^2\phi_D}{128\pi^5 N\eta^4} \int_0^\infty F_D(\lambda)\epsilon_A(\lambda)\lambda^4 d\lambda \quad (5)$$

R_0 is highly dependent on the overlap integral, which expresses the degree of spectral overlap between the donor emission spectra and the acceptor absorption spectra. The quantum yield of the fluorescent species, ϕ_D , the refractive index of the medium, η , and an orientation factor, κ^2 , describing the orientation of the transition dipoles for the donor and acceptor are other parameters in the R_0 . N is Avogadro's number. For these systems, ϕ_D is estimated as 0.03,¹⁴ κ^2 is 0.667 for randomly oriented transition dipoles (this value is typically chosen for FRET calculations and will lead to an error of not more than 35%), and η for CH_2Cl_2 is 1.4212.¹⁵

11. J. V. Caspar, T. J. Meyer, *J. Am. Chem. Soc.*, 1983, **105**, 5583-5590.

12. P. Chen, T. J. Meyer, *Chem Rev.*, 1998, **98**, 1439-1477.

13. J. R. Lackowicz, In *Principles of Fluorescence Spectroscopy*; Kluwer Academic/Plenum; New York, 1999, pg 367-374.

14. Capser, J. V.; Meyer, T. J. *Inorg. Chem.* **1983**, 22, 2444-2453.

15. Marcus, Y. In *Ion Solvation*; John Wiley and Sons, Inc.: Chichester, 1985, pp 136-137.

The spectral overlap between the absorption profile of [Fc] complexes and emission profile of [Ru] complexes is shown in Figure S7. The FRET rate was determined by application of Eq 4 to each set of D–A dyads. Values of τ_f for **Ru^A** and **Ru^B** are reported in Table 1 of the manuscript and are 0.84 and 1.24 μs respectively. The radius, r , of Eq 4 between the donor [Ru] and acceptor [Fc] species are approximated by geometric radii of each component as it contributes to the D–A separation through the hydrogen bonded interface: $r = r_{\text{Ru}} + r_{\text{Fc}}$, where $r_{\text{Ru}} = 6 \text{ \AA}$ (for both **Ru^A** and **Ru^B**), $r_3 = 3.2 \text{ \AA}$, $r_5 = 7.3 \text{ \AA}$, and $r_9 = 7.3 \text{ \AA}$. The FRET radius, R_0 , is calculated using Eq 5 with the parameters listed above. The overlap integral, J , was calculated using the emission spectra of **Ru^A** and **Ru^B** and absorption spectra for **3**, **5**, **9**, (Figure S7) for each D–A dyad plotted on an energy axis (ordinate being cm^{-1}). Comparison between calculated FRET rates and the observed quenching rates reveals that the predicted FRET rates are more than two orders of magnitude smaller than the observed quenching rates. The limitation for FRET in these systems is due to the negligible overlap integral between [Fc] absorption spectra and [Ru] emission spectra.

Table S1. Results for Steady-State Emission Spectra Fits using Single Mode Franck-Condon Analysis at 280K and λ_o determined for fitting Variable-temperature Emission Spectra

Dyad	E_{00}/cm^{-1} ^a	$\hbar\omega_M/\text{cm}^{-1}$ ^a	$\Delta\bar{\nu}_{0,1/2}/\text{cm}^{-1}$ ^a	S_M ^a	λ_o/eV ^b	λ_M/eV ^c	$\Delta G^\circ_{\text{es}}/\text{eV}$
Ru^A:Ph-am	15,200	1300	1790	0.42	0.12	0.10	2.04
Ru^A:3	15,200	1080	1700	0.56	0.10	0.10	2.03
Ru^B:Ph-am	16,600	1911	1420	0.58	0.11	0.09	2.13
Ru^B:3	16,700	1470	1330	0.81	0.05	0.10	2.16

^a fitted parameters determined from spectral fitting of steady-state emission spectra to Eq 1. ^b determined from the slope of a linear fit to the data in Figure 2 as expressed in Eq 3 in text. ^c $\lambda_M = S_M \cdot \hbar\omega_M$.

Table S2. Förster Energy Transfer Parameters and Calculated Rate

	3:Ru^A	5:Ru^A	9:Ru^A	3:Ru^B	5: Ru^B	9: Ru^B
$\tau_f \times 10^6 / \text{sec}$	0.84	0.84	0.84	1.24	1.24	1.24
$r \times 10^{-8} / \text{cm}$	9.20	13.3	11.5	9.20	13.3	11.5
$J \times 10^{-14} / \text{cm}^6 \text{mole}^{-1}$	0.89	2.56	4.98	1.34	3.41	8.41
$R_0^6 \times 10^4 / \text{Å}$	5.32	13.0	32.1	5.79	14.7	36.2
$k_{\text{FRET}}(\text{calc}) \times 10^4 \text{s}^{-1}$	1.01	2.71	1.60	7.58	2.11	1.24
$k_{\text{obs}} \times 10^4 \text{s}^{-1}$	448.	330.	238.	179.	521.	345.

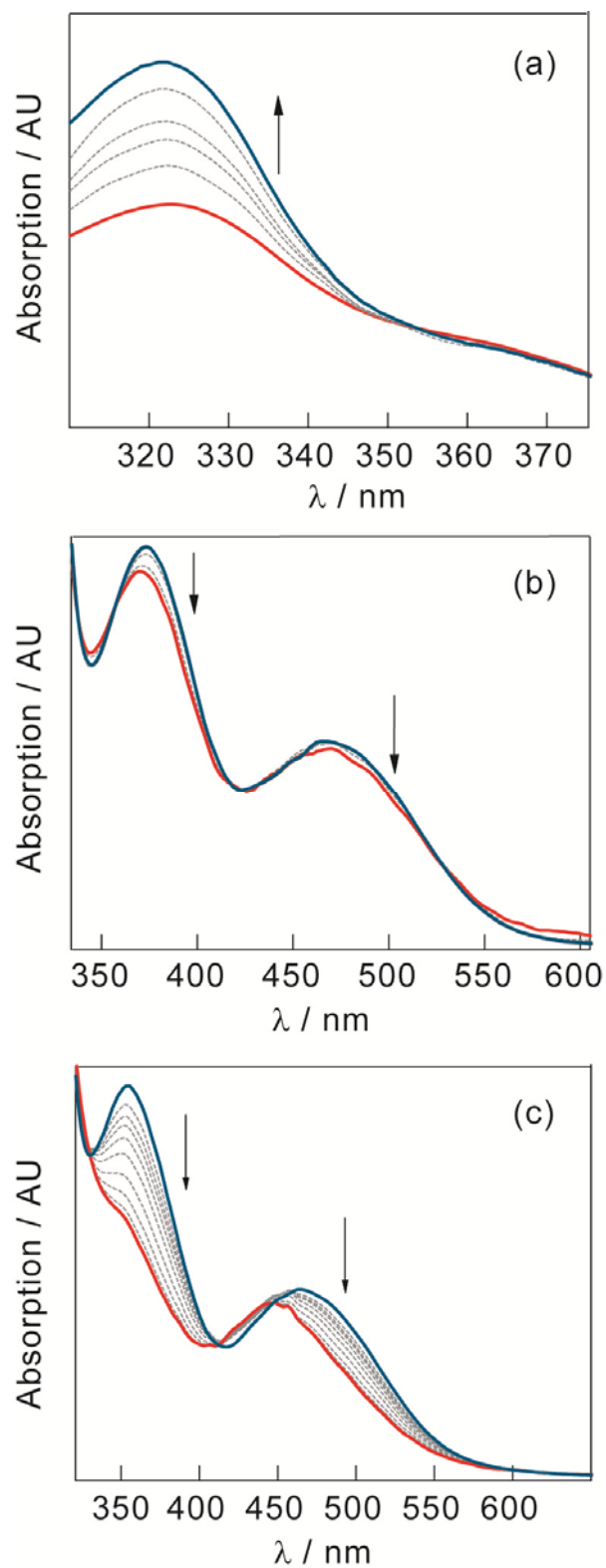


Figure S1. Spectral shifts associated with deprotonation of the amidinium of (a) **3**, (b) **5** and (c) **9** with DMAP in CH₃CN at room temperature.

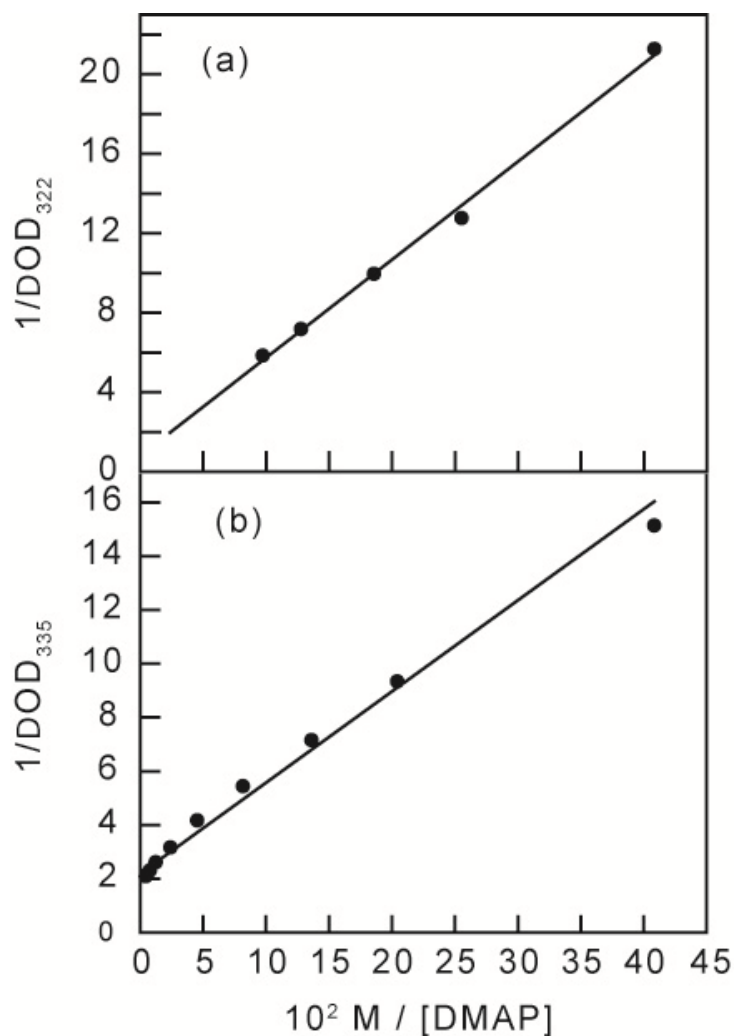


Figure S2. Benesi-Hildebrand plots ($1/\Delta A_{\text{MLCT}}$ vs. $1/[\text{DMAP}]$) for spectral shifts of (a) **3** (slope = 0.0034; y -intercept = 2.19; $K_a' = 6.44 \times 10^2$) and (b) **9** (slope = 0.0049; y -intercept = 0.807; $K_a' = 1.65 \times 10^2$) upon deprotonation of amidinium using 4-dimethylamino-pyridine (DMAP). Data taken from absorptions spectra of Figure S1. Absorption spectra of **3** were corrected for the contribution of DMAP absorption in the high energy spectral region owing to a DMAP absorption tail that extends to 320 nm.

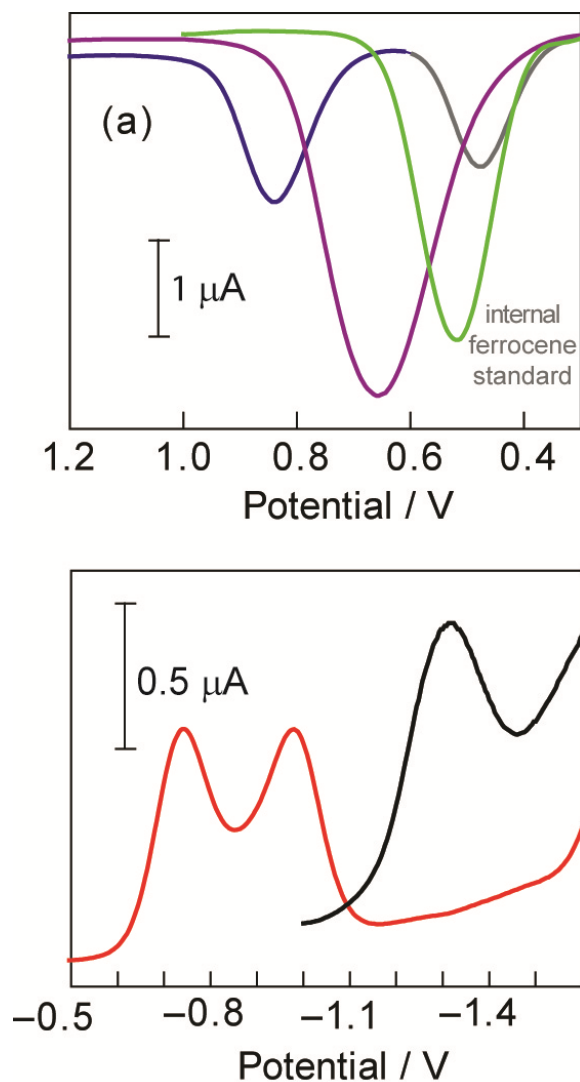


Figure S3. Differential Pulse Voltammetry (DPV) for **Ru^A**, **Ru^B**, **3**, **5**, and **9** in dichloromethane. Potentials, E_p , for each compound (vs Fc^+/Fc) are: $E_p(\mathbf{3}) = 0.84 \text{ V}$ (—); $E_p(\mathbf{5}) = 0.66 \text{ V}$ (—); $E_p(\mathbf{9}) = 0.51 \text{ V}$ (—); $E_p(\mathbf{Ru}^{\text{A}}) = -0.74 \text{ V}$ (—); $E_p(\mathbf{Ru}^{\text{B}}) = -1.33 \text{ V}$ (—). Reduction and oxidation potentials are determined versus a Ag/AgCl reference electrode in CH_2Cl_2 with 0.1 M $(\text{Bu}_4\text{N})\text{ClO}_4$ electrolyte solution.

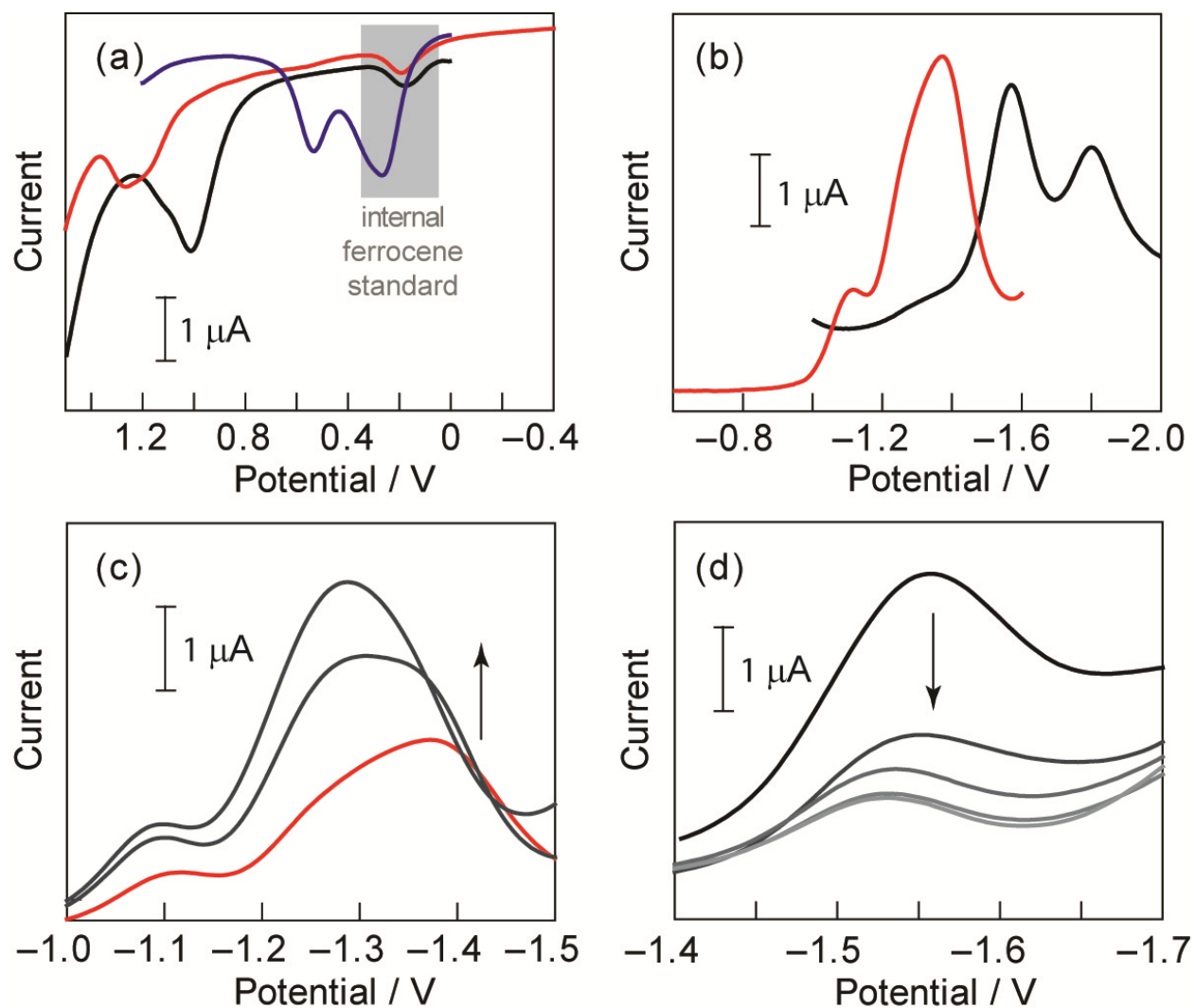


Figure S4. Differential Pulse Voltammograms (DPV) of **Ru^A**, **Ru^B**, **3** in THF with 0.1 M (Bu₄N)PF₆ electrolyte. (A) Oxidation potentials (vs Ag/AgCl) of $E_p(\mathbf{Ru}^A) = 1.27$ eV (—); $E_p(\mathbf{Ru}^B) = 1.01$ eV (—); and $E_p(\mathbf{3}) = 0.54$ eV (—). (B) Reduction potentials (vs Fc⁺/Fc) of $E_p(\mathbf{Ru}^A) = -1.11$ eV (—) and $E_p(\mathbf{Ru}^B) = -1.57$ eV (—). (C) Addition of phenylamidine (**Ph-am**) up to 30 eq excess of **Ru^A** results in only a 24 mV increase in E_p . (D) Addition of **Ph-am** up to 50 eq excess of **Ru^B** results in only a 30 mV increase in E_p .

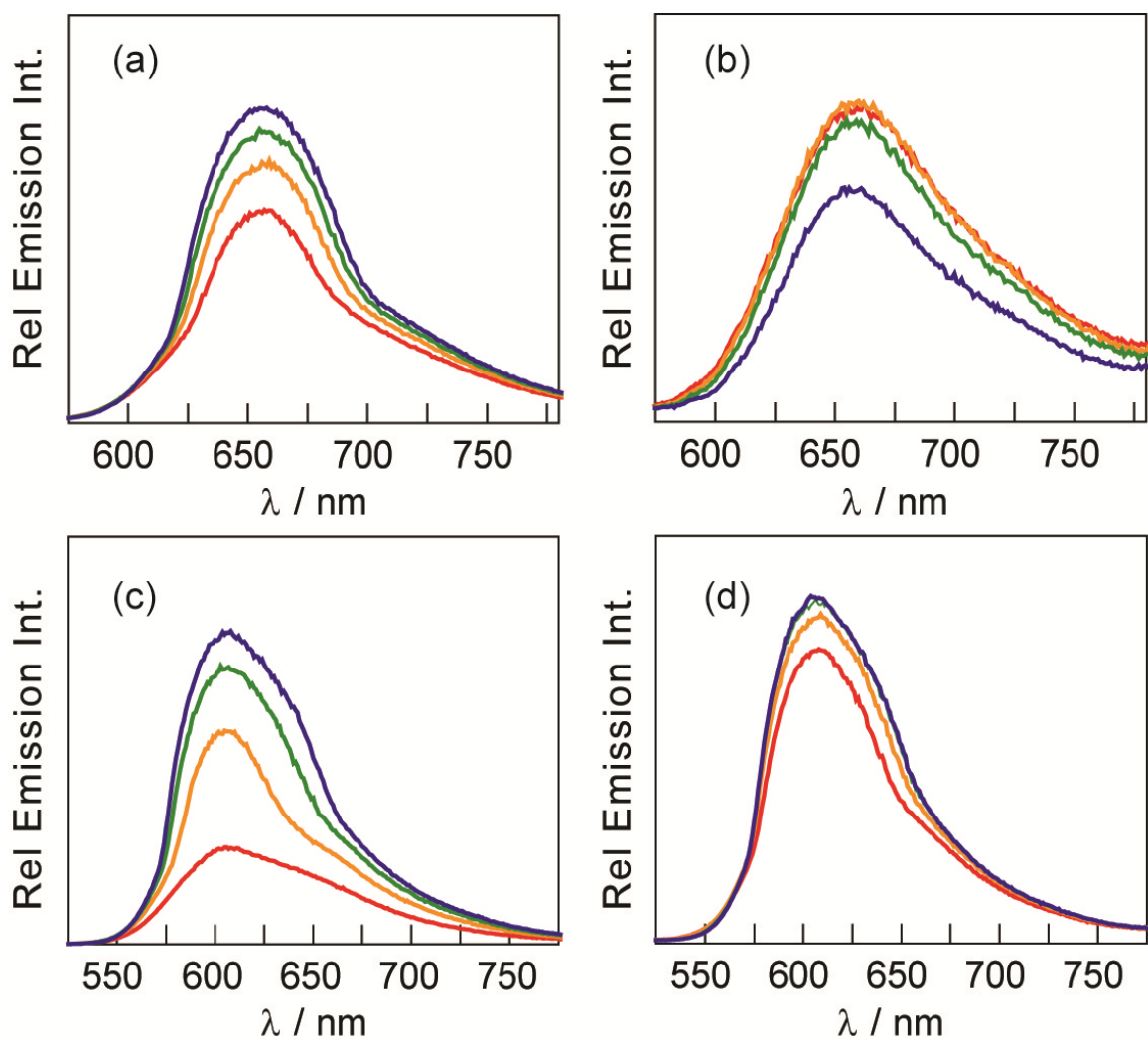


Figure S5. Variable-temperature (—, 240 K; —, 260 K; —, 280 K; —, 300 K) emission spectra of (a) **Ru^A:Ph-am**; (b) **Ru^A:3**; (c) **Ru^B:Ph-am** and **Ru^B:3** at 1×10^{-4} M in [Ru] complex and 10 equiv of **3** or **Ph-am**: For **Ru^A:3**, 5 equiv of **3** was used as significant quenching occurred at higher equiv of **3**, hindering efficient collection of the emission spectra.

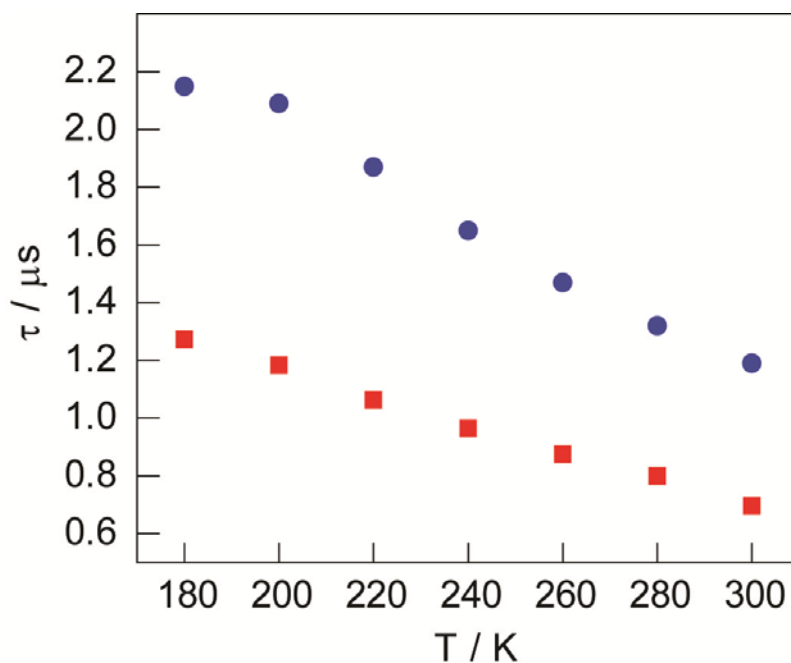


Figure S6. Plot of the lifetime versus temperature for unbound **Ru^A** (■) and **Ru^B** (●) in CH_2Cl_2 upon 400 nm excitation. Samples are prepared at 1×10^{-4} M and lifetime decays obeyed a monoexponential functional form.

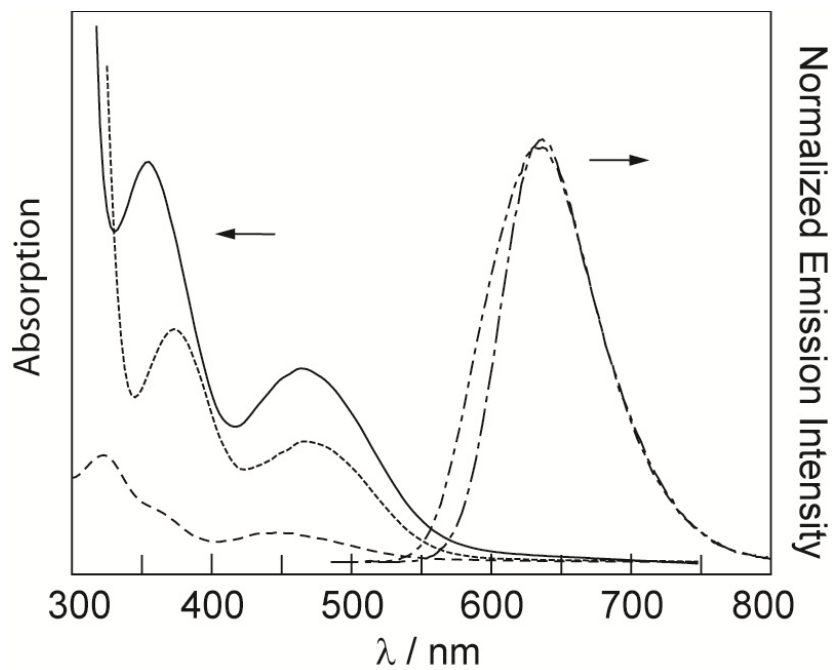


Figure S7. Spectral overlap between absorption spectra of **3** (---), **5** (----) and **9** (—) and the emission spectra of **Ru^A** (—•—) and **Ru^B** (-•-•-).